Journal of Integrative Neuroscience

J. Integr. Neurosci. **2026**; 25(1): 47508
https://doi.org/10.31083/JIN47508

Original Research

Association of Functional and White Matter Structural Brain Network in Older Cerebral Small Vessel Disease With Cognitive Impairment

Yumeng Gu[1,†], Jing Zhao[1,†], Wenjun Feng[1], Chao Wang[2], Yu Yan[1], Xiaowen Wang[3], Xin Li[1,*]

[1]Department of Neurology, Second Hospital of Tianjin Medical University, 300211 Tianjin, China
[2]Department of Health and Medical/Geriatrics, Second Hospital of Tianjin Medical University, 300211 Tianjin, China
[3]Department of Neurology, First Affiliated Hospital of Tianjin University of Traditional Chinese Medicine, 300073 Tianjin, China
*Correspondence: lixinsci@126.com (Xin Li)
[†]These authors contributed equally.
Academic Editor: Simona Lattanzi
Submitted: 1 July 2025 Revised: 28 November 2025 Accepted: 8 December 2025 Published: 23 January 2026

Abstract

Background: To investigate topological brain network properties, intra- and inter-network network patterns, rich-club organization, structural-functional coupling, and their associations with cognitive impairment in elderly patients with cerebral small vessel disease (CSVD). **Methods**: A total of 264 participants were enrolled: 60 healthy controls, 93 CSVD patients without mild cognitive impairment (CSVD-NMCI), and 111 CSVD patients with MCI (CSVD-MCI). All underwent neuropsychological testing and multimodal magnetic resonance imaging (MRI). Structural and functional networks were constructed, and graph theory was applied to assess global and local topology. Associations among network metrics, default mode network (DMN), frontoparietal control network (FPCN), dorsal attention network (DAN), rich-club connectivity, structural connectivity (SC)–functional connectivity (FC) coupling, and cognitive scores were examined. **Results**: CSVD patients exhibited significant global and nodal topological disruption ($p < 0.05$, Bonferroni correction). In CSVD-MCI, FC was reduced within the DMN and DAN but increased within the FPCN. FC within the DAN and between DMN–DAN was positively correlated with Auditory Verbal Learning Test (AVLT) performance. SC-FC coupling was significantly higher in CSVD-MCI than in CSVD-NMCI and controls ($p < 0.05$). Rich-club, feeder, and local connections were markedly impaired in CSVD-MCI and correlated with AVLT and Symbol Digit Modalities Test scores. **Conclusions**: CSVD is associated with decreased network efficiency and elevated SC-FC coupling. Altered FC in the FPCN, DMN, and DAN may indicate compensatory mechanisms, whereas rich-club disruption may be key evidence for cognitive impairment. These findings provide novel insights into network dysfunction underlying cognitive decline in CSVD.

Keywords: cerebral small vessel disease; diffusion tensor imaging; magnetic resonance imaging; mild cognitive impairment

1. Introduction

The prevalence of cerebrovascular disorders has steadily increased, largely in parallel with the growing burden of vascular risk factors in aging populations. Within this spectrum, cerebral small vessel disease (CSVD) has emerged as a leading contributor to neurological disability. Epidemiological data suggest that CSVD accounts for roughly one-quarter of ischemic strokes and nearly half of dementia cases worldwide [1]. Since the disease often develops insidiously and may remain clinically silent for years, CSVD-related mild cognitive impairment (MCI) is frequently overlooked. White-matter changes have been linked to decreased cognition in individuals with metabolic and vascular risk profiles, indicating that clusters of subclinical vascular insults may accelerate cerebrovascular damage [2]. If these patients are not identified and managed at an early stage, progressive deterioration may lead to overt dementia, imposing a substantial socioeconomic and caregiving burden. Therefore, a better understanding of the mechanisms underlying cognitive dysfunction in CSVD is essential to enable earlier detection, institute preventive strategies, and improve clinical outcomes.

Normal brain function relies on the dynamic interplay among multiple large-scale networks, each specialized for different cognitive roles [3]. The default mode network (DMN) is primarily active during rest and inward-focused processing [4], while the dorsal attention network (DAN) facilitates attention to external stimuli and task-related demands [5]. The frontoparietal control network (FPCN) is believed to interact with either the DMN or DAN, depending on the context, providing top-down regulation across diverse cognitive processes [6,7]. Although DMN alterations have been reported in CSVD, much less is known about how CSVD affects the DAN and FPCN, or the interactions among these networks. Examining both within- and between-network interactions among the DMN, DAN, and FPCN could provide valuable information on the neural mechanisms underlying cognitive deficits in CSVD.

In the brain's network organization, highly linked hub regions establish a densely interconnected "rich-club".

These nodes constitute a high-capacity backbone that facilitates efficient long-range communication and integration across distributed systems [8]. Rich-club organization is now recognized as a fundamental property of the connectome, and accumulating evidence indicates that disturbances in this core network are a common feature of diverse neurologic and psychiatric diseases [9]. However, it is still debated whether CSVD predominantly produces diffuse network disruption or whether damage is relatively concentrated in the rich-club and its associated pathways.

Advanced magnetic resonance imaging (MRI) methods enable the measurement of both structural and functional brain networks. In graph-theoretical models, structural connectivity (SC) captures anatomical fiber pathways, whereas functional connectivity (FC) reflects the temporal synchrony of activity between regions [10]. With advances in multimodal MRI, SC-FC coupling—an index integrating structural and functional information—has become a useful tool for evaluating the integrity of brain networks [11–14]. Prior work on SC-FC coupling has mainly focused on gray-matter nodes. However, demyelination and small-vessel-related white-matter damage are hallmark MRI features of CSVD and are closely tied to clinical outcomes. Evaluating SC-FC coupling with an emphasis on white-matter networks may therefore reveal additional mechanisms linking CSVD to impaired cognition.

In this study, we used graph-theoretical analysis to systematically examine alterations in structural and functional brain networks in older adults with CSVD. We further examined intra- and inter-network FC within the DMN, DAN, and FPCN, and examined rich-club organization in all participants. In addition, we investigated SC-FC coupling to explore the relationship between anatomical connectivity and functional synchrony. In addition, we analyzed the associations between network metrics and cognitive performance to provide insights into the neuroanatomical mechanisms underlying cognitive impairment in CSVD.

2. Methods

2.1 Subjects

Participants were enrolled from the Neurology Department and the Physical Examination Center at the Second Hospital of Tianjin Medical University. Between January 2021 and December 2023, 398 individuals were initially screened.

All enrolled patients were diagnosed with sporadic CSVD. Inclusion criteria for CSVD participants were as follows: (1) age between 50 and 80 years; (2) at least 6 years of formal education; (3) MRI evidence of CSVD according to standards for reporting vascular changes on neuroimaging-2 (STRIVE-2) criteria [15], including: (i) white matter hyperintensities (WMH) graded using the Fazekas scale (0–3) on T2-weighted Fluid Attenuated Inversion Recovery (T2-FLAIR) [16]; (ii) lacunes (3–15 mm) in subcortical regions with cerebrospinal fluid—like signals on T1-Weighted Imaging (T1WI) and T2-FLAIR; (iii) cerebral microbleeds (CMBs) assessed using the Microbleed Anatomical Rating Scale (MARS) [17]; and (iv) enlarged perivascular spaces (EPVS) evaluated by Maclullich's method [18]; (4) a total CSVD burden score (0–4) based on the presence of lacunes, CMBs, severe WMH (Fazekas 3 periventricular or 2–3 deep WMH), and moderate-to-severe EPVS in the basal ganglia [19]; (5) informed consent form signed by participants.

MCI was defined according to the Vascular Behavioral and Cognitive Disorders (VASCOG) criteria for vascular cognitive impairment [20]: (1) evidence of acquired decline in one or more cognitive domains compared with previous functioning, based on informant or clinician report and/or standardized testing (approximately 1–2 SD below normative means); and (2) preservation of independence in basic and instrumental activities of daily living, although tasks may require more time, effort or compensatory measures. The specific cognitive domains assessed are provided in **Supplementary Data 1**.

Exclusion criteria included: (1) individuals with known or suspected monogenic CSVD (e.g., Cerebral Autosomal Dominant Arteriopathy with Subcortical Infarcts and Leukoencephalopathy [CADASIL], Cerebral Autosomal Recessive Arteriopathy with Subcortical Infarcts and Leukoencephalopathy [CARASIL], or other hereditary small-vessel syndromes) were excluded based on clinical history, family history, and characteristic MRI findings inconsistent with sporadic CSVD; (2) major neurological or psychiatric disorders; (3) non-vascular causes of white matter lesions; (4) large cortical or non-lacunar infarcts; (5) cardioembolic stroke; (6) $\geq$50% stenosis of intracranial or extracranial arteries; (7) substance abuse; (8) severe aphasia or physical disability precluding assessment; (9) inability to tolerate MRI; (10) Hamilton Depression Rating Scale-17 (HDRS-17) $\geq$8 [21]; or (11) Generalized Anxiety Disorder-7 (GAD-7) $\geq$5 [22].

Control participants met the following criteria: (1) at least 6 years of education; (2) no history of stroke or serious systemic disease; (3) Fazekas score $\leq$1 with no significant structural abnormalities on MRI; (4) HDRS-17 $<$8; (5) GAD-7 score 0–4; and (6) normal cognitive test results.

After excluding participants due to incomplete clinical data (n = 32), abnormal neurological examinations (n = 23), refusal or inability to undergo MRI (n = 31), inability to cooperate with cognitive assessments (n = 27), or excessive head motion (n = 21), the final sample comprised 60 controls, 93 CSVD without MCI (CSVD-NMCI) and 111 CSVD with MCI (CSVD-MCI) (Fig. 1).

2.2 Neuropsychological Assessment

Before MRI scanning, all participants completed standardized cognitive testing. Cognitive function was assessed using the Chinese version of the Montreal Cognitive Assessment (MoCA), which has been validated for language

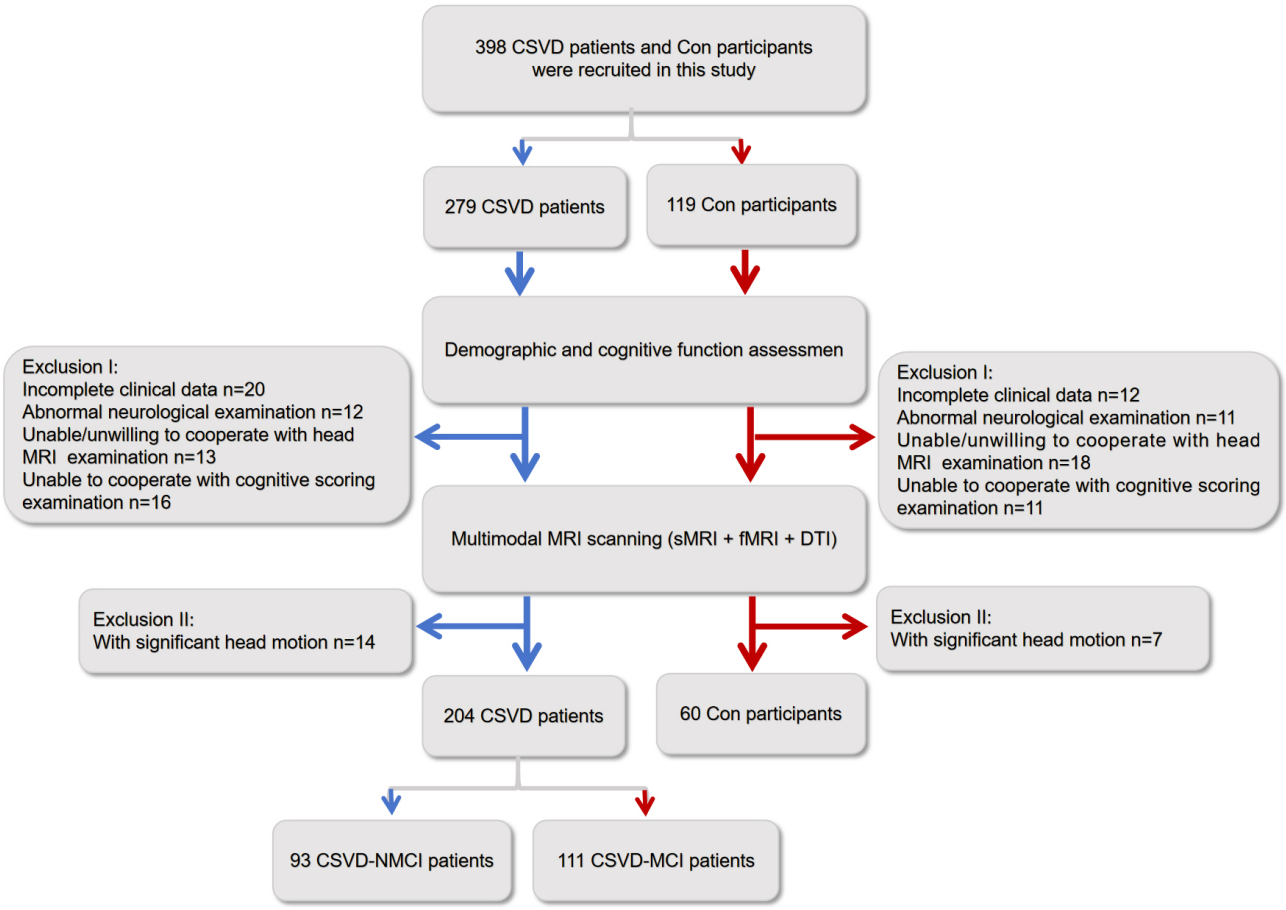

Fig. 1. Overview of participant recruitment and exclusion for CSVD patients and controls. CSVD, cerebral small vessel disease; DTI, diffusion tensor imaging; CSVD-MCI, CSVD patients with mild cognitive impairment; CSVD-NMCI, CSVD patients without mild cognitive impairment; Con, control group; MRI, magnetic resonance imaging; sMRI, structural magnetic resonance imaging; fMRI, functional magnetic resonance imaging.

and cultural appropriateness [23]. One additional point was added for participants with $\leq$12 years of education; MoCA scores between 18 and 26 were classified as consistent with MCI [24]. Episodic memory was evaluated using the Auditory Verbal Learning Test (AVLT) and the delayed recall score of the Rey-Osterrieth Complex Figure Test (ROCF) [25]. Working memory was measured with the Digit Span (DS) test [26]. Visuospatial abilities were assessed with the ROCF copy score [27] and Clock Drawing Test (CDT) [28]. Executive function was examined using the Stroop Color-Word Test (SCWT-C-B) and the Color Trails Test Part B (CTT-B) [29]. Language abilities were measured using the Boston Naming Test (BNT) and the Verbal Fluency Test (VFT) [30]. Attention and processing speed were evaluated with the Symbol Digit Modalities Test (SDMT) and the Color Trails Test, Part A (CTT-A) [31].

2.3 Nuclear Magnetic Resonance Data Acquisition

All MRI data were collected on a 3.0 T GE scanner (Signa HDxt; GE HealthCare, Chicago, IL, USA) equipped with a 32-channel head coil. The imaging protocol included resting-state fMRI (rs-fMRI), diffusion tensor imaging (DTI), high-resolution T1-weighted scans, and T2-FLAIR sequences. DTI was performed with 32 diffusion directions, b = 1000 s/mm^2, reference b = 0, repetition time (TR) = 8000 ms, echo time (TE) = 88.4 ms, matrix = 128 $\times$ 128, field of view (FOV) = 256 $\times$ 256 mm^2, 75 slices, and 2 mm slice thickness without gaps. Rs-fMRI used TR = 2000 ms, TE = 30 ms, flip angle = 90°, FOV = 240 $\times$ 240 mm^2, matrix = 64 $\times$ 64, 3 mm slices, over 8.6 minutes. T1-weighted scans had TR = 8.2 ms, TE = 3.2 ms, 1 mm slice thickness, matrix = 256 $\times$ 256, and flip angle = 12°. T2-FLAIR imaging was acquired with TR = 9075 ms, TE = 150 ms, inversion time (TI) = 2250 ms, FOV = 256 mm^2, and 160 slices.

2.4 Nuclear Magnetic Resonance Data Preprocessing

Rs-fMRI: Preprocessing was performed with the DPARSF toolbox (DPABI_V8.2_240510; http://rfmri.org/dpabi) [32], including removal of the first 10 volumes, slice-timing adjustment, motion correction, spatial normalization, smoothing, and band-pass filtering.

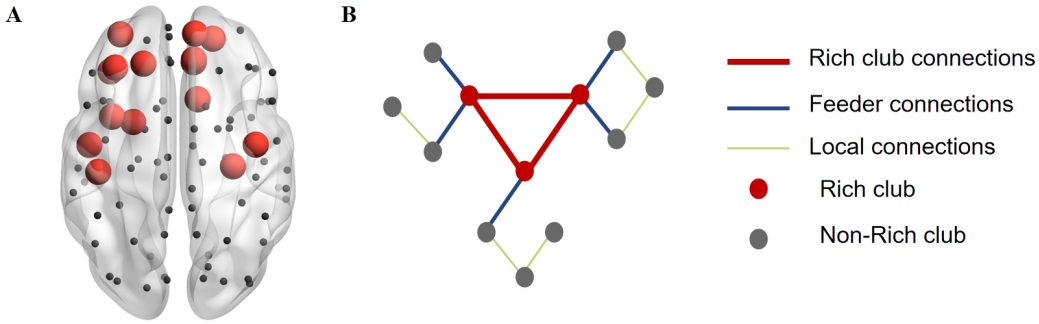

Fig. 2. Schematic illustration of local, feeder, and rich-club connections. (A) Rich-club nodes (red) and peripheral regions (black) identified across all groups. (B) Classification of structural network connections. For each category—rich-club, feeder, and local—the overall "connection strength" was computed as the sum of the edge weights within that group.

DTI: Diffusion data were processed using the PANDA toolbox (PANDA_1.3.1; https://www.nitrc.org/frs/?group_id=582) [33]. The pipeline included brain extraction (BET), eddy-current and motion correction, tensor fitting, and registration to a standard template. Additional methodological details are provided in the **Supplementary Material-Method**.

2.5 Construction of Brain Networks

A total of 90 cortical and subcortical regions of interest (ROIs) were delineated based on the Automated Anatomical Labeling (AAL) atlas, with the cerebellum excluded [34]. For functional networks, pairwise Pearson correlations of blood oxygen level dependent (BOLD) time series between ROIs were computed to generate 90 × 90 FC matrices. Structural networks were constructed from DTI-derived fiber number matrices (90 × 90). Graph theory measures were computed using the GRETNA (https://www.nitrc.org/projects/gretna/) [35]. Complete information on network construction is provided in the **Supplementary Material-Method**.

2.6 Graph Theory Analysis

The network measures encompassed clustering coefficient (Cp), characteristic path length (Lp), global efficiency (Eglob), local efficiency (Elocal), and small-worldness ($\sigma = \gamma/\lambda$). Nodal properties included degree, efficiency, and betweenness centrality. All metrics were calculated across a sparsity range of 0.10–0.30 in 0.01 increments, with the area under the curve (AUC) employed for group comparisons [36]. Complete information on network topological attributes is provided in the **Supplementary Table 1**.

2.7 Total Intracranial Volume Analysis

T1-weighted scans were analyzed with CAT12 and SPM12 within MATLAB R2012b (MathWorks, Natick, MA, USA). Volumes of gray matter, white matter, and cerebrospinal fluid were extracted. WMH volume was normalized as a percentage of total intracranial volume using the formula: WMH volume/total intracranial volume × 100%.

2.8 Rich-Club Organization of Structural Network

Rich-club nodes were identified as the highest-degree 15% of regions, determined by averaging node degree across all subjects [37]. This subset comprised PreCG.R, SFGdor.L, ORBsup.R, MFG.L, ORBmid.L, ORBinf.L, ROL.L, OLF.R, SFGmed.R, REC.R, INS.L, ACG.R, HIP.R, PoCG.L, and PUT.L (Fig. 2A; **Supplementary Data 2**) [38]. Based on the separation of rich-club and non-rich-club regions, the structural network was divided into three types of connections: (i) connections linking rich-club regions (red), (ii) pathways joining rich-club regions with peripheral regions (blue), and (iii) connections confined to peripheral regions (green) (Fig. 2B).

2.9 Definition of Resting State Network

The DMN, FPCN, and DAN were delineated using a seed-based region-of-interest strategy. Following the procedures outlined by Grady *et al.* [39] and Spreng *et al.* [40], 5-mm-radius spheres were placed at previously published Montreal Neurological Institute (MNI) coordinates. In line with established descriptions [41], the DMN set encompassed bilateral posterior cingulate cortex (PCC), medial prefrontal areas, the inferior parietal complex, lateral temporal regions, and the hippocampal formation. The FPCN was represented by bilateral dorsolateral prefrontal cortex (DLPFC), dorsomedial prefrontal zones, and lateral parietal cortex, while the DAN consisted of bilateral intraparietal sulcus, frontal eye field regions, and middle temporal loci [42,43]. For each seed, the average BOLD signal was obtained, and correlation coefficients were calculated for every ROI pair.

For every participant, six connectivity indices were calculated: three reflecting internal coherence within the DMN, FPCN, and DAN, and three capturing interactions among the DMN–FPCN, DMN–DAN, and FPCN–DAN pairs. These measures were compared with cognitive performance scores to evaluate their functional significance. Further methodological details are presented in the **Supplementary Material-Method**.

Table 1. Demographics and neuropsychological tests of all participants.

Variable	Con (N = 60)	CSVD-NMCI (N = 93)	CSVD-MCI (N = 111)	F/x^2	p
	Mean (SD)/Median (IQR) or No. (%)	Mean (SD)/Median (IQR) or No. (%)	Mean (SD)/Median (IQR) or No. (%)		
Age (year)	64.86 (6.442)	65.20 (7.068)	65.87 (6.411)	0.516	0.598
Male	31 (51.7)	52 (55.9)	54 (48.6)	1.072	0.585
BMI (kg/m^2)	27.082 (3.150)	26.986 (3.656)	27.302 (3.694)	0.209	0.811
Education level				5.541	0.236
Below High School	33 (55.0)	37 (39.8)	60 (54.1)		
High School	16 (26.7)	37 (39.8)	32 (28.8)		
High school or above	11 (18.3)	19 (20.4)	19 (17.1)		
Systolic pressure (mm Hg)	138.211 (16.409)	137.245 (16.005)	136.720 (17.568)	0.154	0.857
Diastolic pressure (mm Hg)	80.772 (9.398)	78.820 (10.333)	78.538 (10.261)	1.027	0.359
Vascular risk factors					
Hypercholesterolemia (%)	13 (21.7)	22 (23.7)	25 (22.5)	0.087	0.958
Diabetes Mellitus (%)	14 (23.3)	27 (29.0)	40 (36.0)	3.139	0.208
Hypertension (%)	29 (48.3)	46 (49.5)	62 (55.9)	1.223	0.542
History of Drinking				1.761	0.780
Never drank alcohol	46 (76.7)	67 (72.0)	77 (69.4)		
Previous Drinking	2 (3.3)	7 (7.5)	8 (7.2)		
Drinking now	12 (20.0)	19 (20.4)	26 (23.4)		
Smoking history				1.564	0.815
Never smoked	40 (66.7)	56 (60.2)	64 (57.7)		
Previous smoking	5 (8.3)	11 (11.8)	12 (10.8)		
Smoking now	15 (25.0)	26 (28.0)	35 (31.5)		
Neuropsychological assessment					
MoCA	27.30 (0.763)	26.91 (2.492)	22.98 (4.427)	82.170	$0.000^{b,c}$
AVLT delayed recall	6 (5, 9)	6 (4, 8)	5 (3, 8)	10.199	0.006^{b}
ROCF delay	27.851 (3.934)	27.604 (3.595)	27.217 (4.125)	0.568	0.568
DS positive sequence	7.86 (1.928)	7.45 (1.635)	7.18 (1.831)	2.827	0.061
DS reverse order	4 (3, 5)	4 (3, 5)	4 (3, 4)	1.300	0.522
ROCF copy	34.82 (2.110)	34.76 (2.236)	34.38 (3.062)	0.789	0.455
CDT	2.50 (0.875)	2.26 (0.973)	2.43 (0.916)	1.436	0.240
SCWT-C-B	12 (5, 23)	13 (5, 20)	12 (6, 19)	0.011	0.994
CTT-B	146.2 (115, 211.3)	150 (113.4, 205.3)	150 (116.9, 199.3)	0.249	0.883
BNT	14.25 (1.044)	14.14 (1.217)	14.20 (1.063)	0.185	0.832
VFT	15.33 (4.388)	14.28 (4.906)	14.95 (4.785)	0.990	0.373
SDMT	29.5 (22, 36)	29 (20, 34)	26 (15, 33)	8.765	0.012^{b}
CTT-A	93.2 (66.0, 131.6)	92.1 (68.3, 136.6)	94.2 (70.3, 125.1)	0.343	0.842

b: Con vs. CSVD-MCI; c: CSVD-NMCI vs. CSVD-MCI; Covariance: Age, gender, education level, and vascular risk factors. IQR, interquartile range; BMI, body mass index; MoCA, Montreal Cognitive Assessment; AVLT, Auditory Verbal Learning Test; ROCF, Rey-Osterrieth Complex Figure Test; DS, Digit Span; CDT, Clock Drawing Test; SCWT-C-B, Stroop Color-Word Test; CTT-B, Color Trails Test Part B; BNT, Boston Naming Test; VFT, Verbal Fluency Test; SDMT, Symbol Digit Modalities Test; CTT-A, Color Trails Test Part A.

2.10 SC-FC Coupling Analysis

SC-FC coupling was quantified by correlating the vectorized structural and functional connectivity matrices, producing an individual-level measure of correspondence between physical pathways and functional interactions. A full description of the computation process is available in the **Supplementary Material-Method**.

2.11 Statistical Analysis

Demographic, clinical, and cognitive data were processed in SPSS version 22.0 (IBM Corp., Armonk, NY, USA). The Shapiro–Wilk test was applied to evaluate distributional assumptions. For measures meeting normality criteria, group differences in demographic factors and neuropsychological performance were examined using ANCOVA, followed by Bonferroni-adjusted post hoc comparisons. For non-normally distributed data, the Kruskal–Wallis test was applied, followed by Dunn's test for post hoc inter-group comparisons, with Bonferroni-adjusted p-values. Categorical variables were analyzed using chi-square tests. Pearson correlation analyses were performed to evaluate relationships between network measures and cognitive scores, controlling for age, sex, education, mood scales, and vascular risk factors (VRFs). A two-tailed $p < 0.05$ was considered statistically significant.

3. Results

3.1 Demography and Neuropsychological Data

The three groups—controls, CSVD-NMCI, and CSVD-MCI—did not differ significantly in age, sex, educational background, or vascular risk factors ($p > 0.05$). However, significant group effects emerged for cognitive measures, including MoCA scores, AVLT delayed recall, and SDMT performance ($p < 0.05$). Comprehensive demographic and neuropsychological data are summarized in Table 1.

3.2 Neuroimaging Findings in Patients With CSVD

No significant differences were detected between CSVD-NMCI and CSVD-MCI groups in total CSVD burden, imaging features, or brain volume normalized to intracranial volume (Table 2).

3.3 Functional and Structural Network Analysis

3.3.1 Small-World Properties and Network Global Efficiency Analysis

All three groups demonstrated small-world organization in both structural and functional networks ($\gamma > 1$, $\lambda \approx 1$, $\sigma > 1$). Within the structural network, the CSVD-MCI group exhibited lower γ and higher λ compared with controls, while the CSVD-NMCI group showed elevated λ relative to controls. Compared with the CSVD-NMCI group, the CSVD-MCI group had reduced γ and σ. In addition, the CSVD-NMCI group displayed decreased Eglob, Elocal, and Cp compared with controls. The CSVD-MCI group, relative to controls, also showed lower Elocal and Cp along with higher Lp (Fig. 3; **Supplementary Table 2**).

Within the functional network, individuals in the CSVD-MCI group showed higher λ and lower γ and σ relative to healthy controls. When compared with the CSVD-NMCI group, the only notable alteration was an elevation in λ. The CSVD-MCI group also displayed reduced Eglob and Elocal and a longer Lp in relation to controls. In contrast to the CSVD-NMCI group, they exhibited a marked decline in Elocal (Fig. 4; **Supplementary Table 2**).

3.3.2 Analysis of Network Node Efficiency

In the structural network analysis, patients with CSVD-MCI showed markedly reduced centrality in the left superior temporal gyrus (STG.L), a lower node degree in the left middle frontal gyrus (MFG.L), right postcentral gyrus (PoCG.R), and left precentral gyrus (PCG.L), as well as diminished node efficiency in the MFG.L and both hippocampi (HIP.L, HIP.R), compared with controls. Compared with the CSVD-NMCI group, individuals in the CSVD-MCI group showed a lower node degree in the left anterior cingulate gyrus (ACG.L) and decreased nodal efficiency in the MFG.L (Fig. 5A; **Supplementary Table 3**).

Within the functional network, the CSVD-NMCI group exhibited lower centrality in the PCG.L compared with controls. The CSVD-MCI group, relative to controls, showed reduced centrality in the left inferior orbitofrontal gyrus (ORBinf.L) and PCG.L, decreased node degree in the left amygdala (AMYG.L) and left calcarine gyrus (CAL.L), and diminished nodal efficiency in the right supplementary motor area (SMA.R). Compared with the CSVD-NMCI group, the CSVD-MCI group demonstrated further reduction in nodal efficiency of the SMA.R (Fig. 5B; **Supplementary Table 3**).

3.3.3 Functional Network: Intra-Network FC and Inter-Network FC

Intra-network FC of the DMN and DAN was significantly lower in the CSVD-MCI group compared with controls. Controls also exhibited stronger FC in these networks than the CSVD-NMCI group ($p < 0.05$, Dunn test, Bonferroni-corrected; Fig. 6A). In CSVD-MCI participants, FC within the DAN showed a positive correlation with AVLT scores ($r = 0.223$, $p = 0.019$; Fig. 6B).

Regarding inter-network connectivity, functional coupling between the FPCN and DMN was significantly elevated in the CSVD-MCI group compared with controls ($p < 0.05$, ANCOVA, Bonferroni-corrected; Fig. 6C). In CSVD-MCI participants, greater FPCN–DMN connectivity was inversely correlated with AVLT performance ($r = -0.241$, $p = 0.011$; Fig. 6D).

Table 2. Neuroimaging findings of CSVD patients.

	CSVD-NMCI (N = 93)	CSVD-MCI (N = 111)	*p*-value
Total CSVD Burden			0.221
Grade 1, n (%)	61 (65.6)	84 (75.7)	
Grade 2, n (%)	22 (23.7)	14 (12.6)	
Grade 3, n (%)	9 (9.7)	11 (9.9)	
Grade 4, n (%)	1 (1.1)	2 (1.8)	
Cerebrovascular lesions			
Fazekas classification			0.187
WMH Fazekas 0–1, n (%)	12 (12.9)	22 (19.8)	
WMH Fazekas 2–3, n (%)	81 (87.1)	89 (80.2)	
Lacunes occurrence, n (%)	28 (30.1)	33 (29.7)	0.953
CMBs occurrence, n (%)	16 (17.2)	21 (18.9)	0.752
EPVS occurrence, n (%)	11 (11.8)	10 (9.0)	0.509
Neuroimaging measures			
Total GMV, mean (SD)	32.66 (2.21)	32.25 (1.63)	0.130
Total WMV, mean (SD)	26.33 (2.95)	26.55 (2.30)	0.550
Total WMHV, mean (SD)	3.75 (1.20)	3.45 (1.18)	0.074

Covariance: Age, gender, education level, and vascular risk factors. WMH, white matter hyperintensities; CMBs, cerebral microbleeds; EPVS, enlarged perivascular spaces; GMV, gray matter volume; WMV, white matter volume; WMHV, white matter hyperintensity volume.

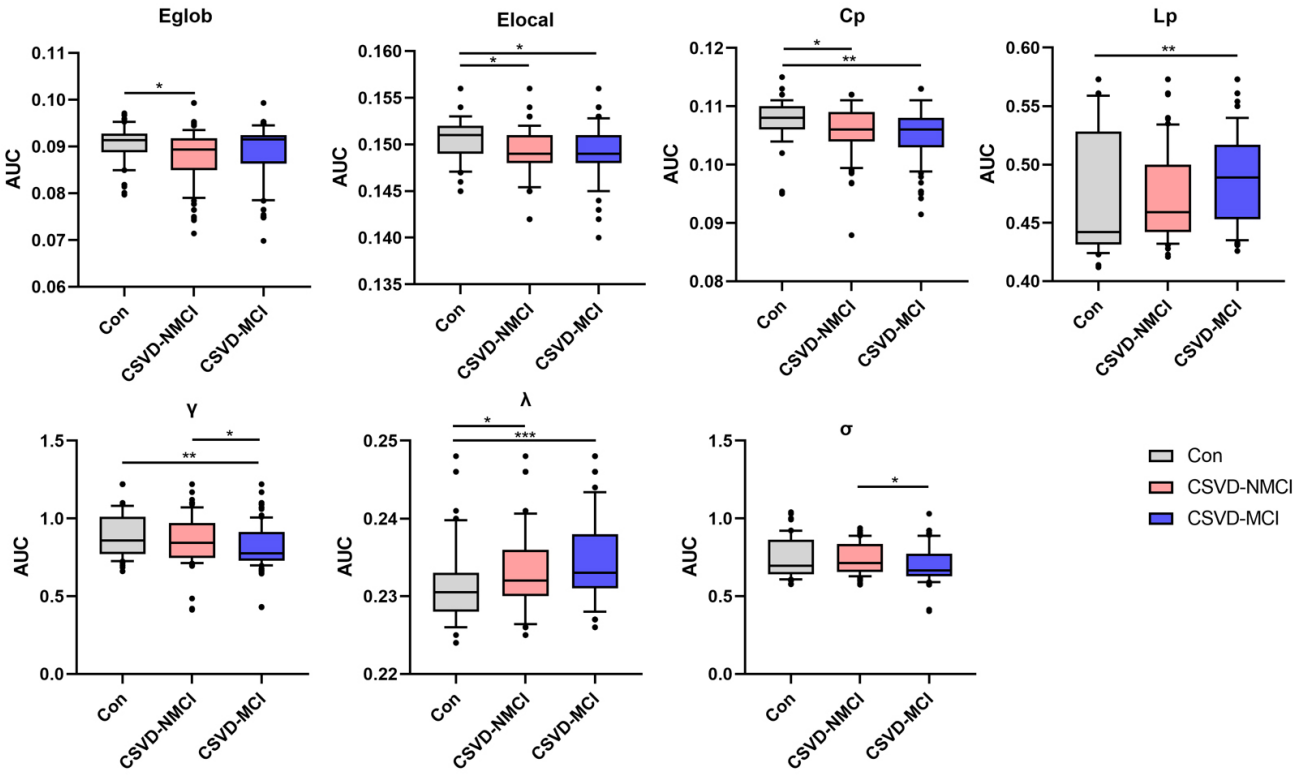

Fig. 3. Group differences in global white-matter network metrics, evaluated using AUC values. Statistical comparisons were conducted with the Dunn test, with significance set at $p < 0.05$ after Bonferroni correction. AUC, area under the curve; Cp, clustering coefficient; Lp, characteristic path length; Eglob, global efficiency; Elocal, local efficiency. *$p < 0.05$, **$p < 0.01$, ***$p < 0.001$.

3.3.4 Structural Network: Rich-Club Organization

Rich-club connectivity showed significant intergroup differences (ANCOVA, $p < 0.05$, controlling for age, gender, and education level). The control group had the highest connection strength, followed by CSVD-NMCI, while CSVD-MCI patients had the lowest connection strength ($p < 0.05$, Bonferroni correction). Compared with the Con group, the feeder pathway contributions of CSVD-MCI pa-

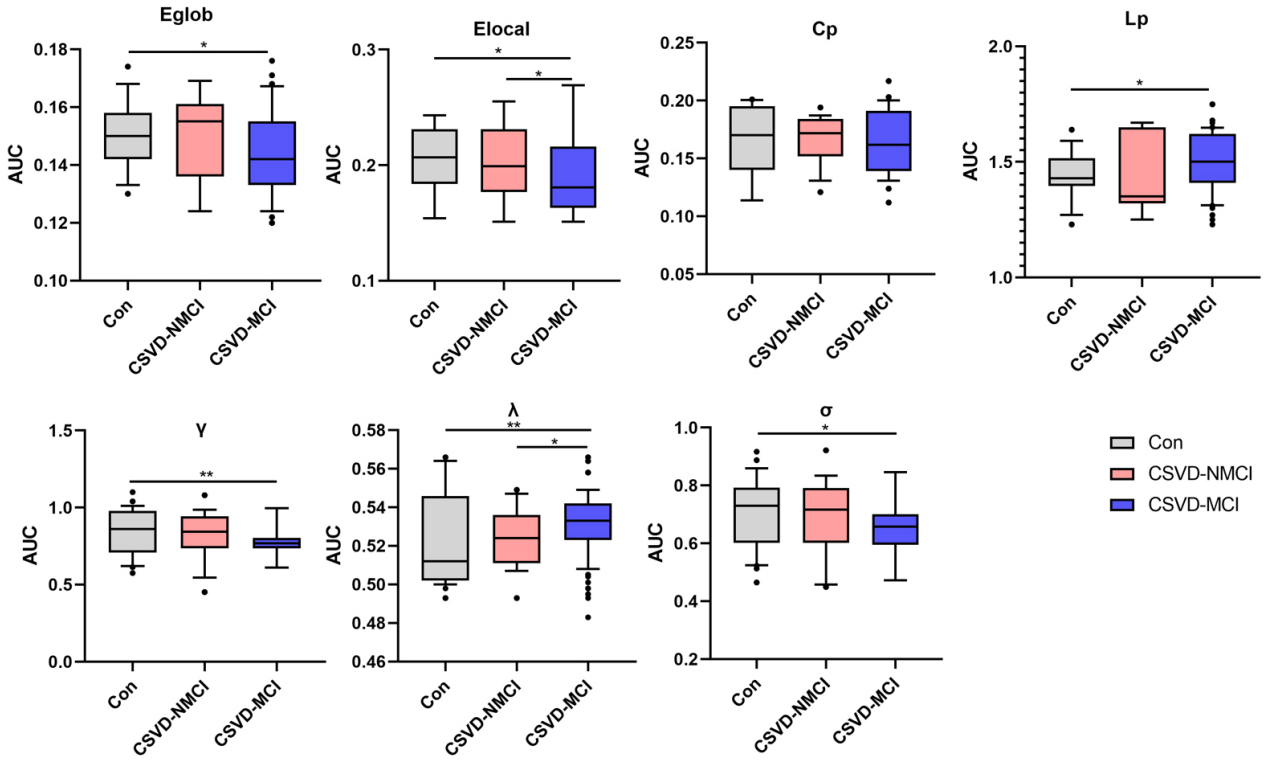

Fig. 4. Comparison of global parameters of functional networks among groups was performed using AUC values. Group differences were assessed using Dunn test, with $p < 0.05$ considered statistically significant, after Bonferroni correction. *$p < 0.05$, **$p < 0.01$.

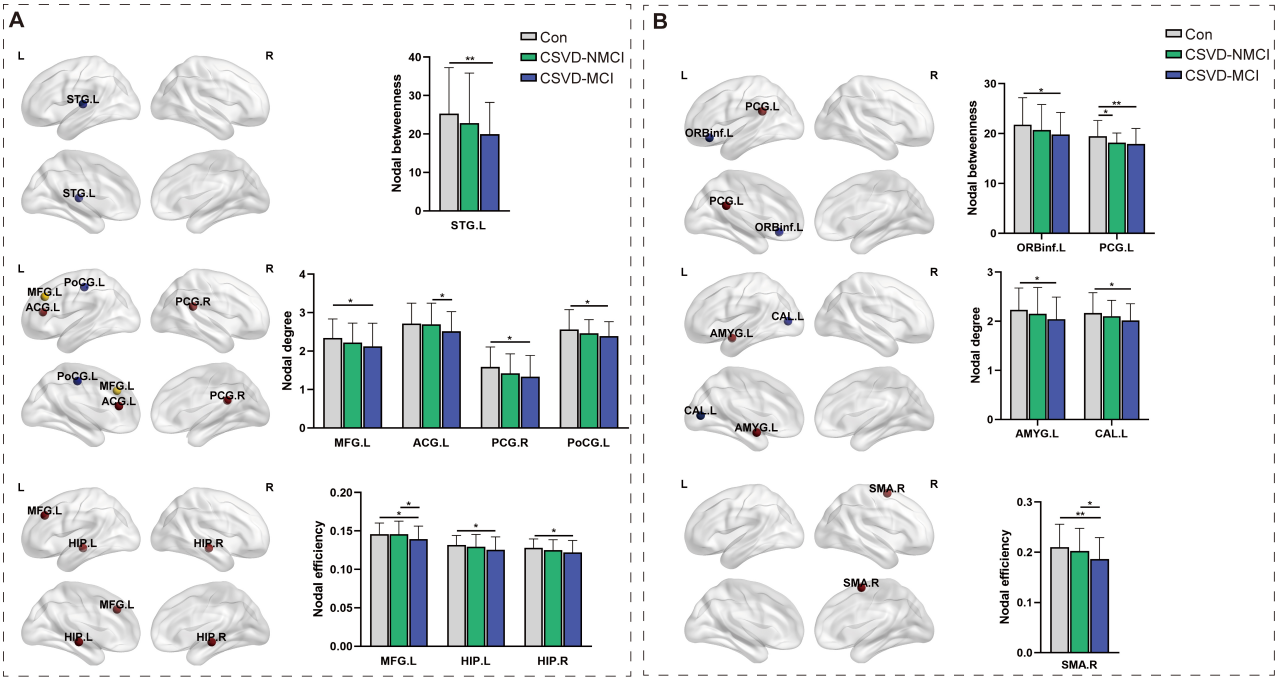

Fig. 5. Comparison of node-level network metrics across groups. (A) Structural network. (B) Functional network. STG.L, left superior temporal gyrus; MFG.L, left middle frontal gyrus; ACG.L, left anterior cingulate gyrus; AMYG.L, left amygdala; CAL.L, left calcarine gyrus; SMA.R, right supplementary motor area; PCG.L, left precentral gyrus; PCG.R, right precentral gyrus; PoCG.L, left postcentral gyrus; HIP.L, left hippocampus; HIP.R, right hippocampus; ORBinf.L, left inferior orbitofrontal gyrus. *$p < 0.05$, **$p < 0.01$.

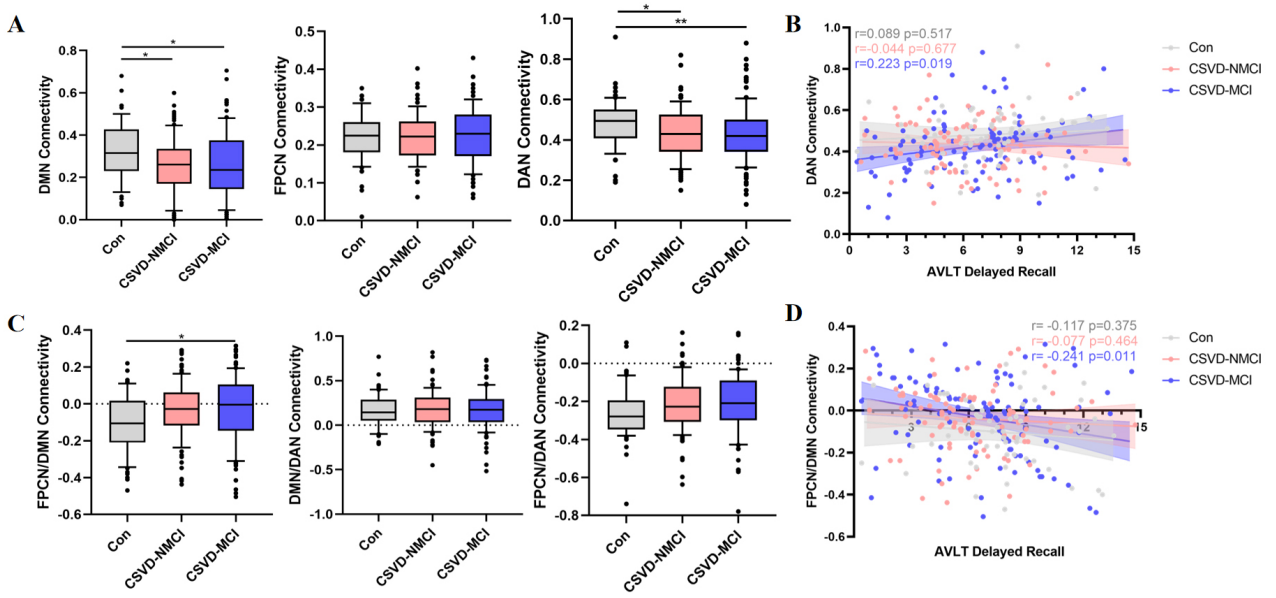

Fig. 6. Comparison of functional networks between intra network and inter network. (A) Differences in FC intra-network among groups. (B) Correlation between AVLT scores and intra-network connectivity measures. (C) Differences in FC inter-network among groups. (D) Correlation between AVLT scores and inter-network connectivity measures. FC, functional connectivity; DMN, default mode network; FPCN, frontoparietal control network; DAN, dorsal attention network. *$p < 0.05$, **$p < 0.01$.

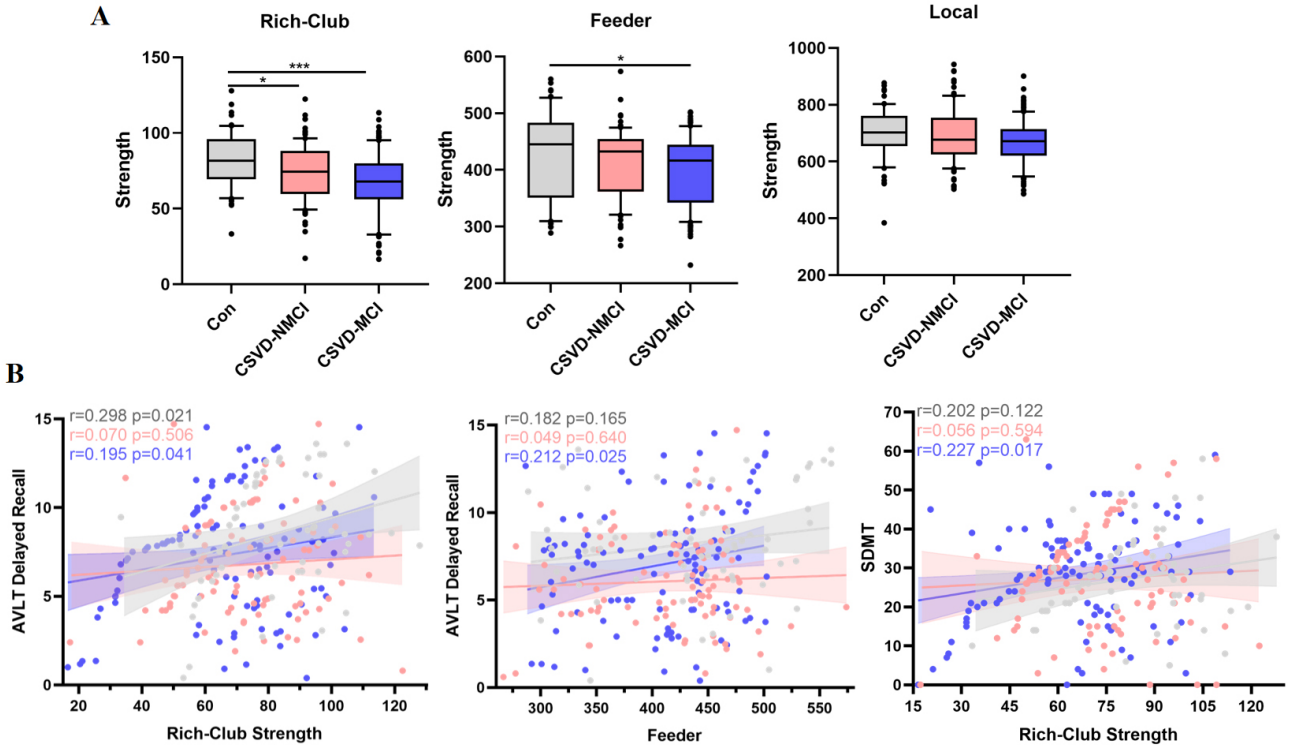

Fig. 7. Comparison of rich-hub organization in the structural network. (A) Group differences in the strength of rich-club, feeder, and local pathways. (B) Associations between these connectivity metrics and cognitive performance. Each dot reflects one participant. The solid line represents the regression fit, and the shaded band denotes the 95% confidence interval. Partial correlation coefficients (r) and corresponding *p*-values are provided (FDR-corrected). FDR, false discovery rate. *$p < 0.05$, ***$p < 0.001$.

tients were significantly reduced (Dunn test, $p < 0.05$, Bonferroni correction) (Fig. 7A).

We evaluated the associations between connectivity strength and cognitive performance separately within

the control, CSVD-NMCI, and CSVD-MCI groups. For the AVLT, rich-club connection strength correlated with performance in both the control and CSVD-MCI groups, while feeder connection strength was significantly related to AVLT in CSVD-MCI. In the SDMT, only rich-club strength in CSVD-MCI showed a significant association (Fig. 7B; false discovery rate [FDR]-corrected $p < 0.05$).

3.3.5 Altered SC-FC Coupling and Relationship to All Rich-Club Organization

Significant group differences were observed in SC-FC coupling across all connections ($F = 6.165$, $p = 0.002$), rich-club connections ($F = 3.496$, $p = 0.032$) (ANCOVA, controlling for age, sex, education and vascular risk factors; Bonferroni correction applied), and feeder connections ($z = 7.975$, $p = 0.019$) (Dunn test, Bonferroni correction applied).

SC-FC coupling was elevated in the CSVD-MCI group relative to controls (ANCOVA, $p = 0.002$). In addition, SC-FC coupling was significantly increased for rich-club connections (ANCOVA, control vs. CSVD-MCI: $p < 0.001$; CSVD-NMCI vs. CSVD-MCI: $p = 0.044$). Feeder connections also demonstrated increased coupling in the CSVD-MCI group compared with controls (Dunn test, $p = 0.015$) (Fig. 8A).

After adjusting for age, sex, and education, partial correlation analysis showed that SC-FC coupling was positively related to rich-club connection strength in both the control group ($r = 0.449$, $p < 0.001$) and the CSVD-MCI group ($r = 0.229$, $p = 0.016$; Fig. 8B).

4. Discussion

Our results suggest that, although structural and functional networks retain small-world properties, CSVD—particularly when accompanied by MCI—is associated with a shift toward less optimal network organization. Reduced γ and σ together with increased λ in CSVD-MCI suggest a move toward a more randomized topology, implying decreased global integration and less efficient transfer of information [44]. Comparable alterations in small-world architecture have been documented in conditions such as major depressive disorder, schizophrenia, and Alzheimer's disease [36,45,46].

Patients with CSVD-NMCI showed relatively preserved small-world indices and efficiency, suggesting that large-scale network architecture may remain intact during the early CSVD stages. In contrast, CSVD-MCI patients displayed more pronounced declines in both structural and functional integration, in line with more advanced white-matter injury and altered synchrony of neural activity. Tract-based analyses further showed a stepwise decrease in white-matter fiber density from controls to CSVD-NMCI to CSVD-MCI (**Supplementary Fig. 1**). These results are in agreement with longitudinal data indicating that alterations in structural network organization in CSVD may precede and predict subsequent cognitive deterioration or transition to dementia [47]. These findings highlight the importance of detecting brain network disruption early in the course of the disease.

Our study found that FC within the DMN and DAN was significantly reduced in CSVD-MCI patients. Reduced connectivity between the FPCN and DMN was also observed, which was significantly correlated with AVLT performance. The DAN supports attention to external stimuli [48], whereas the DMN plays a key role in episodic memory [49]. The FPCN appears to function as a bridge, coordinating with both the DMN and DAN to facilitate goal-directed cognitive processes [50]. In this context, reduced intra-network connectivity in DMN and DAN, combined with increased FPCN-DMN coupling that was negatively associated with memory performance, may reflect a maladaptive reorganization in which additional control resources are recruited but fail to fully compensate for underlying damage. Even though overall CSVD burden scores were comparable between the CSVD-NMCI and CSVD-MCI groups, selective damage to periventricular and deep frontal white-matter pathways linked to the FPCN and DMN may underlie the reduced network efficiency and associated impairments in memory.

Rich-club brain regions consist of highly interconnected nodes that support efficient communication within the network [51]. The superior frontal gyrus, middle frontal gyrus, hippocampus, thalamus, and putamen have been consistently identified as rich-club nodes [52]. Due to their central role in network topology, connections among these rich-club nodes are essential for integrating information across distant brain regions [53]. Damage to rich-club connections has a greater impact on global network efficiency than random network disruptions [3]. In our CSVD-MCI cohort, rich-club connections showed the greatest reduction in strength, whereas feeder and local connections were relatively less affected. Simultaneously, SC-FC coupling involving rich-club and feeder connections was increased, suggesting a heightened dependence on residual structural pathways to maintain functional coherence. These findings align with previous research [3,10,54–56] indicating that disruption of rich-club hubs and their feeder pathways contributes disproportionately to network inefficiency and cognitive decline in CSVD.

SC-FC coupling is increasingly regarded as a sensitive indicator of the interplay between brain structure and function. Reduced SC-FC coupling has been described in several conditions—including stroke, epilepsy, and Alzheimer's disease—indicating disconnection between anatomy and function [13,14,55,57]. In contrast, in the present study, CSVD-MCI patients exhibited significantly increased SC-FC coupling compared with controls. One possible explanation is that this increase represents a maladaptive or over-compensatory response to underlying network disruption. Elevated SC-FC coupling may reflect

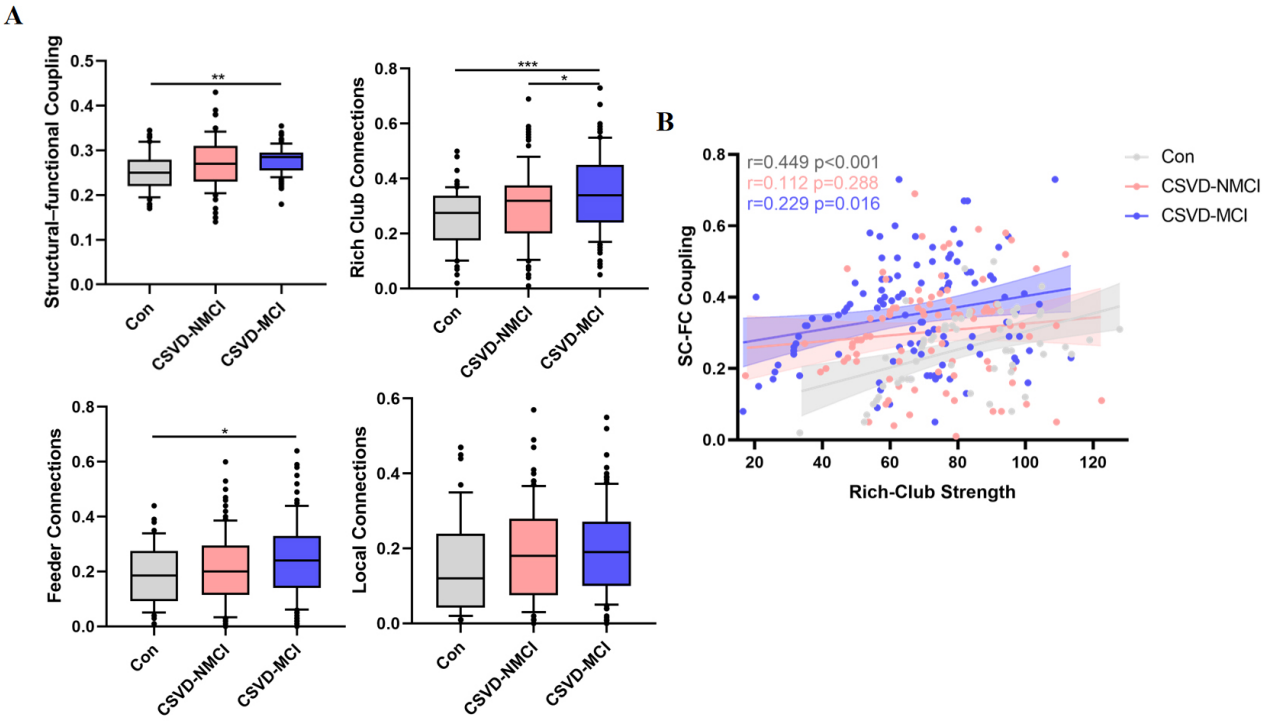

Fig. 8. Comparison of SC-FC coupling. (A) SC-FC coupling levels across the control, CSVD-NMCI, and CSVD-MCI groups. (B) Associations between SC-FC coupling and rich-club connectivity indices (*$p < 0.05$, **$p < 0.01$, ***$p < 0.001$). SC, structural connectivity.

excessive reliance on structurally preserved pathways to maintain function, potentially reducing network flexibility and adaptability [55]. These findings suggest that higher SC-FC coupling does not necessarily indicate optimal network function, particularly in pathological conditions.

Binswanger's disease (subcortical ischemic vascular disease of the Binswanger type) provides an example of CSVD in which extensive white-matter rarefaction and subcortical infarcts are tightly linked to progressive cognitive impairment [58,59]. Although white matter hyperintensities remain the hallmark imaging finding in CSVD, cognitive dysfunction frequently coexists with other MRI markers—including silent lacunar infarcts, cerebral microbleeds, enlarged perivascular spaces, and global or regional brain atrophy—all contributing to the heterogeneous clinical presentation [60]. Therefore, future research should focus on delineating specific neuroimaging subgroups in CSVD, and on exploring how the combination of these imaging markers and lesion topography affects network connectivity, cognitive outcomes, and disease trajectories. This work will help clarify the multifactorial mechanisms of CSVD and support the development of more precise diagnostic and therapeutic strategies.

5. Limitation

This study has several limitations. First, its cross-sectional design precludes causal inference and limits the ability to observe how network organization evolves as CSVD progresses from early asymptomatic stages to mild cognitive impairment and later phases. Longitudinal studies are therefore warranted to delineate the temporal trajectory of structural and functional network alterations. Second, more advanced methods, such as partial correlation or machine learning—based coupling analyses, may provide a more comprehensive characterization of network interactions. Third, although neuroimaging provides valuable insights into macroscopic brain organization, it does not capture the underlying molecular or cellular mechanisms of CSVD. Integrating neuroimaging with multi-omics approaches (e.g., genomics, proteomics, metabolomics) may help elucidate the biological basis of network alterations and cognitive decline. Future work should systematically characterize these subtypes to better understand their distribution and clinical relevance.

6. Conclusions

In conclusion, elderly patients with CSVD, particularly those with MCI, show impaired efficiency and integrity of both structural and functional networks related to cognition. These alterations manifest as slower and less efficient information transfer, reduced robustness, and diminished neural processing resources. Changes in FC within and between the FPCN, DMN, and DAN likely represent a mixture of compensatory and maladaptive reorganization in response to small-vessel-related damage. Disproportionate vulnerability of rich-club regions and their connecting path-

ways appears to play a central role in the development of cognitive impairment. Abnormal increases in SC-FC coupling, especially in rich-club-related connections, further highlight the complex restructuring of the brain's communication in CSVD. Together, these findings provide network-based insights into how CSVD contributes to cognitive dysfunction and underscore the need for early detection and targeted interventions.

Availability of Data and Materials

The data that support the findings of this study are available from the corresponding author upon reasonable request.

Author Contributions

YG—Software, Validation, Writing-Original Draft. JZ—Investigation, Data Curation. WF—Data Curation, Project administration, Resources, Funding acquisition. CW—Formal analysis. YY—Data Curation, Project administration. XW—Methodology, Writing-Review & Editing. XL—Conceptualization, Resources, Writing-Review & Editing, Supervision, Funding acquisition. All authors contributed to editorial changes in the manuscript. All authors read and approved the final manuscript. All authors have participated sufficiently in the work and agreed to be accountable for all aspects of the work.

Ethics Approval and Consent to Participate

Ethical approval was granted by the ethics committee of The Second Hospital of Tianjin Medical University, KY2020K183. All legal guardians or appropriate representatives of the participants have provided informed consent form on their behalf. All methods involving human participants were performed in accordance with the ethical standards of the institutional research committee and the 1964 Helsinki declaration and its later amendments or comparable ethical standards.

Acknowledgment

We acknowledge the hard work and dedication of all non-author staff involved in implementing the study's intervention and evaluation components.

Funding

This work was sponsored by the Tianjin scientific and technological project (25JCQNJC00780), the National Natural Science Foundation of China (42275197) and the Key Discipline of Geriatric Medicine in Tianjin (TJYXZDXK-3-017C).

Conflict of Interest

The authors declare no conflict of interest.

Supplementary Material

Supplementary material associated with this article can be found, in the online version, at https://doi.org/10.31083/JIN47508.

References

[1] Cannistraro RJ, Badi M, Eidelman BH, Dickson DW, Middlebrooks EH, Meschia JF. CNS small vessel disease: A clinical review. Neurology. 2019; 92: 1146–1156. https://doi.org/10.1212/WNL.0000000000007654.

[2] Segura B, Jurado MA, Freixenet N, Bargalló N, Junqué C, Arboix A. White matter fractional anisotropy is related to processing speed in metabolic syndrome patients: a case-control study. BMC Neurology. 2010; 10: 64. https://doi.org/10.1186/1471-2377-10-64.

[3] Tuladhar AM, Lawrence A, Norris DG, Barrick TR, Markus HS, de Leeuw FE. Disruption of rich club organisation in cerebral small vessel disease. Human Brain Mapping. 2017; 38: 1751–1766. https://doi.org/10.1002/hbm.23479.

[4] Broeders TAA, van Dam M, Pontillo G, Rauh V, Douw L, van der Werf YD, *et al*. Energy Associated With Dynamic Network Changes in Patients With Multiple Sclerosis and Cognitive Impairment. Neurology. 2024; 103: e209952. https://doi.org/10.1212/WNL.0000000000209952.

[5] Mallas EJ, De Simoni S, Scott G, Jolly AE, Hampshire A, Li LM, *et al*. Abnormal dorsal attention network activation in memory impairment after traumatic brain injury. Brain: a Journal of Neurology. 2021; 144: 114–127. https://doi.org/10.1093/brain/awaa380.

[6] Deck BL, Kelkar A, Erickson B, Erani F, McConathey E, Sacchetti D, *et al*. Individual-level functional connectivity predicts cognitive control efficiency. NeuroImage. 2023; 283: 120386. https://doi.org/10.1016/j.neuroimage.2023.120386.

[7] Yang W, Xu X, Wang C, Cheng Y, Li Y, Xu S, *et al*. Alterations of dynamic functional connectivity between visual and executive-control networks in schizophrenia. Brain Imaging and Behavior. 2022; 16: 1294–1302. https://doi.org/10.1007/s11682-021-00592-8.

[8] van Norden AGW, de Laat KF, van Dijk EJ, van Uden IWM, van Oudheusden LJB, Gons RAR, *et al*. Diffusion tensor imaging and cognition in cerebral small vessel disease: the RUN DMC study. Biochimica et Biophysica Acta. 2012; 1822: 401–407. https://doi.org/10.1016/j.bbadis.2011.04.008.

[9] Crossley NA, Mechelli A, Scott J, Carletti F, Fox PT, McGuire P, *et al*. The hubs of the human connectome are generally implicated in the anatomy of brain disorders. Brain: a Journal of Neurology. 2014; 137: 2382–2395. https://doi.org/10.1093/brain/awu132.

[10] Ter Telgte A, van Leijsen EMC, Wiegertjes K, Klijn CJM, Tuladhar AM, de Leeuw FE. Cerebral small vessel disease: from a focal to a global perspective. Nature Reviews. Neurology. 2018; 14: 387–398. https://doi.org/10.1038/s41582-018-0014-y.

[11] Wang YF, Gu P, Zhang J, Qi R, de Veer M, Zheng G, *et al*. Deteriorated functional and structural brain networks and normally appearing functional-structural coupling in diabetic kidney disease: a graph theory-based magnetic resonance imaging study. European Radiology. 2019; 29: 5577–5589. https://doi.org/10.1007/s00330-019-06164-1.

[12] Ma J, Liu F, Yang B, Xue K, Wang P, Zhou J, *et al*. Selective Aberrant Functional-Structural Coupling of Multiscale Brain Networks in Subcortical Vascular Mild Cognitive Impairment. Neuroscience Bulletin. 2021; 37: 287–297. https://doi.org/10.1007/s12264-020-00580-w.

[13] Zhang R, Shao R, Xu G, Lu W, Zheng W, Miao Q, *et al*. Aberrant

brain structural-functional connectivity coupling in euthymic bipolar disorder. Human Brain Mapping. 2019; 40: 3452–3463. https://doi.org/10.1002/hbm.24608.

[14] Chen Q, Lv H, Wang Z, Wei X, Liu J, Liu F, *et al*. Distinct brain structural-functional network topological coupling explains different outcomes in tinnitus patients treated with sound therapy. Human Brain Mapping. 2022; 43: 3245–3256. https://doi.org/10.1002/hbm.25848.

[15] Duering M, Biessels GJ, Brodtmann A, Chen C, Cordonnier C, de Leeuw FE, *et al*. Neuroimaging standards for research into small vessel disease-advances since 2013. The Lancet. Neurology. 2023; 22: 602–618. https://doi.org/10.1016/S1474-4422(23)00131-X.

[16] Fazekas F, Chawluk JB, Alavi A, Hurtig HI, Zimmerman RA. MR signal abnormalities at 1.5 T in Alzheimer's dementia and normal aging. AJR. American Journal of Roentgenology. 1987; 149: 351–356. https://doi.org/10.2214/ajr.149.2.351.

[17] Gregoire SM, Chaudhary UJ, Brown MM, Yousry TA, Kallis C, Jäger HR, *et al*. The Microbleed Anatomical Rating Scale (MARS): reliability of a tool to map brain microbleeds. Neurology. 2009; 73: 1759–1766. https://doi.org/10.1212/WNL.0b013e3181c34a7d.

[18] Maclullich AMJ, Wardlaw JM, Ferguson KJ, Starr JM, Seckl JR, Deary IJ. Enlarged perivascular spaces are associated with cognitive function in healthy elderly men. Journal of Neurology, Neurosurgery, and Psychiatry. 2004; 75: 1519–1523. https://doi.org/10.1136/jnnp.2003.030858.

[19] Staals J, Makin SDJ, Doubal FN, Dennis MS, Wardlaw JM. Stroke subtype, vascular risk factors, and total MRI brain small-vessel disease burden. Neurology. 2014; 83: 1228–1234. https://doi.org/10.1212/WNL.0000000000000837.

[20] Sachdev P, Kalaria R, O'Brien J, Skoog I, Alladi S, Black SE, *et al*. Diagnostic criteria for vascular cognitive disorders: a VASCOG statement. Alzheimer Disease and Associated Disorders. 2014; 28: 206–218. https://doi.org/10.1097/WAD.0000000000000034.

[21] Chung MH, Chang WP. Correlation between hemoglobin levels and depression in late-stage cancer patients with irritability as mediating variable. European Journal of Oncology Nursing: the Official Journal of European Oncology Nursing Society. 2023; 67: 102414. https://doi.org/10.1016/j.ejon.2023.102414.

[22] Spitzer RL, Kroenke K, Williams JBW, Löwe B. A brief measure for assessing generalized anxiety disorder: the GAD-7. Archives of Internal Medicine. 2006; 166: 1092–1097. https://doi.org/10.1001/archinte.166.10.1092.

[23] Lu J, Li D, Li F, Zhou A, Wang F, Zuo X, *et al*. Montreal cognitive assessment in detecting cognitive impairment in Chinese elderly individuals: a population-based study. Journal of Geriatric Psychiatry and Neurology. 2011; 24: 184–190. https://doi.org/10.1177/0891988711422528.

[24] Jia X, Wang Z, Huang F, Su C, Du W, Jiang H, *et al*. A comparison of the Mini-Mental State Examination (MMSE) with the Montreal Cognitive Assessment (MoCA) for mild cognitive impairment screening in Chinese middle-aged and older population: a cross-sectional study. BMC Psychiatry. 2021; 21: 485. https://doi.org/10.1186/s12888-021-03495-6.

[25] Sohn BK, Hwang JY, Park SM, Choi JS, Lee JY, Lee JY, *et al*. Developing a Virtual Reality-Based Vocational Rehabilitation Training Program for Patients with Schizophrenia. Cyberpsychology, Behavior and Social Networking. 2016; 19: 686–691. https://doi.org/10.1089/cyber.2016.0215.

[26] Frick A, Fay S, Bouazzaoui B, Sauzéon H, Angel L, Vanneste S, *et al*. The respective contribution of cognitive control and working memory to semantic and subjective organization in aging. Psychology and Aging. 2023; 38: 455–467. https://doi.org/10.1037/pag0000752.

[27] Staios M, Nielsen TR, Kosmidis MH, Papadopoulos A, Kokkinias A, Velakoulis D, *et al*. Validity of Visuoconstructional Assessment Methods within Healthy Elderly Greek Australians: Quantitative and Error Analysis. Archives of Clinical Neuropsychology: the Official Journal of the National Academy of Neuropsychologists. 2023; 38: 598–607. https://doi.org/10.1093/arclin/acac091.

[28] Schmidtke K, Olbrich S. The Clock Reading Test: validation of an instrument for the diagnosis of dementia and disorders of visuo-spatial cognition. International Psychogeriatrics. 2007; 19: 307–321. https://doi.org/10.1017/S104161020600456X.

[29] Pantoja-Cardoso A, Aragão-Santos JC, Santos PDJ, Dos-Santos AC, Silva SR, Lima NBC, *et al*. Functional Training and Dual-Task Training Improve the Executive Function of Older Women. Geriatrics (Basel, Switzerland). 2023; 8: 83. https://doi.org/10.3390/geriatrics8050083.

[30] Lu H, Li J, Fung AWT, Lam LCW. Diversity in verbal fluency performance and its associations with MRI-informed brain age matrices in normal ageing and neurocognitive disorders. CNS Neuroscience & Therapeutics. 2023; 29: 1865–1880. https://doi.org/10.1111/cns.14144.

[31] Zhang Q, Zhu M, Huang L, Zhu M, Liu X, Zhou P, *et al*. A Study on the Effect of Traditional Chinese Exercise Combined With Rhythm Training on the Intervention of Older Adults With Mild Cognitive Impairment. American Journal of Alzheimer's Disease and other Dementias. 2023; 38: 15333175231190626. https://doi.org/10.1177/15333175231190626.

[32] Chao-Gan Y, Yu-Feng Z. DPARSF: A MATLAB Toolbox for "Pipeline" Data Analysis of Resting-State fMRI. Frontiers in Systems Neuroscience. 2010; 4: 13. https://doi.org/10.3389/fnsys.2010.00013.

[33] Cui Z, Zhong S, Xu P, He Y, Gong G. PANDA: a pipeline toolbox for analyzing brain diffusion images. Frontiers in Human Neuroscience. 2013; 7: 42. https://doi.org/10.3389/fnhum.2013.00042.

[34] Tzourio-Mazoyer N, Landeau B, Papathanassiou D, Crivello F, Etard O, Delcroix N, *et al*. Automated anatomical labeling of activations in SPM using a macroscopic anatomical parcellation of the MNI MRI single-subject brain. NeuroImage. 2002; 15: 273–289. https://doi.org/10.1006/nimg.2001.0978.

[35] Wang J, Wang X, Xia M, Liao X, Evans A, He Y. GRETNA: a graph theoretical network analysis toolbox for imaging connectomics. Frontiers in Human Neuroscience. 2015; 9: 386. https://doi.org/10.3389/fnhum.2015.00386.

[36] Zhang J, Wang J, Wu Q, Kuang W, Huang X, He Y, *et al*. Disrupted brain connectivity networks in drug-naive, first-episode major depressive disorder. Biological Psychiatry. 2011; 70: 334–342. https://doi.org/10.1016/j.biopsych.2011.05.018.

[37] van den Heuvel MP, Kahn RS, Goñi J, Sporns O. High-cost, high-capacity backbone for global brain communication. Proceedings of the National Academy of Sciences of the United States of America. 2012; 109: 11372–11377. https://doi.org/10.1073/pnas.1203593109.

[38] Yan T, Wang W, Yang L, Chen K, Chen R, Han Y. Rich club disturbances of the human connectome from subjective cognitive decline to Alzheimer's disease. Theranostics. 2018; 8: 3237–3255. https://doi.org/10.7150/thno.23772.

[39] Grady C, Sarraf S, Saverino C, Campbell K. Age differences in the functional interactions among the default, frontoparietal control, and dorsal attention networks. Neurobiology of Aging. 2016; 41: 159–172. https://doi.org/10.1016/j.neurobiolaging.2016.02.020.

[40] Spreng RN, Sepulcre J, Turner GR, Stevens WD, Schacter DL. Intrinsic architecture underlying the relations among the default, dorsal attention, and frontoparietal control networks of the human brain. Journal of Cognitive Neuroscience. 2013; 25: 74–86.

https://doi.org/10.1162/jocn_a_00281.
[41] Bai F, Watson DR, Shi Y, Wang Y, Yue C, YuhuanTeng, *et al*. Specifically progressive deficits of brain functional marker in amnestic type mild cognitive impairment. PloS One. 2011; 6: e24271. https://doi.org/10.1371/journal.pone.0024271.
[42] Seeley WW, Menon V, Schatzberg AF, Keller J, Glover GH, Kenna H, *et al*. Dissociable intrinsic connectivity networks for salience processing and executive control. The Journal of Neuroscience: the Official Journal of the Society for Neuroscience. 2007; 27: 2349–2356. https://doi.org/10.1523/JNEUROSCI.5587-06.2007.
[43] Fox MD, Snyder AZ, Vincent JL, Corbetta M, Van Essen DC, Raichle ME. The human brain is intrinsically organized into dynamic, anticorrelated functional networks. Proceedings of the National Academy of Sciences of the United States of America. 2005; 102: 9673–9678. https://doi.org/10.1073/pnas.0504136102.
[44] Sporns O, Chialvo DR, Kaiser M, Hilgetag CC. Organization, development and function of complex brain networks. Trends in Cognitive Sciences. 2004; 8: 418–425. https://doi.org/10.1016/j.tics.2004.07.008.
[45] Lynall ME, Bassett DS, Kerwin R, McKenna PJ, Kitzbichler M, Muller U, *et al*. Functional connectivity and brain networks in schizophrenia. The Journal of Neuroscience: the Official Journal of the Society for Neuroscience. 2010; 30: 9477–9487. https://doi.org/10.1523/JNEUROSCI.0333-10.2010.
[46] Sanz-Arigita EJ, Schoonheim MM, Damoiseaux JS, Rombouts SARB, Maris E, Barkhof F, *et al*. Loss of 'small-world' networks in Alzheimer's disease: graph analysis of FMRI resting-state functional connectivity. PloS One. 2010; 5: e13788. https://doi.org/10.1371/journal.pone.0013788.
[47] Kovács P, Tóth B, Honbolygó F, Szalárdy O, Kohári A, Mády K, *et al*. Speech prosody supports speaker selection and auditory stream segregation in a multi-talker situation. Brain Research. 2023; 1805: 148246. https://doi.org/10.1016/j.brainres.2023.148246.
[48] Hu L, Wang C, Talhelm T, Zhang X. Distinguishing the neural mechanism of attentional control and working memory in feature-based attentive tracking. Psychophysiology. 2021; 58: e13726. https://doi.org/10.1111/psyp.13726.
[49] Margulies DS, Ghosh SS, Goulas A, Falkiewicz M, Huntenburg JM, Langs G, *et al*. Situating the default-mode network along a principal gradient of macroscale cortical organization. Proceedings of the National Academy of Sciences of the United States of America. 2016; 113: 12574–12579. https://doi.org/10.1073/pnas.1608282113.
[50] Franzmeier N, Göttler J, Grimmer T, Drzezga A, Áraque-Caballero MA, Simon-Vermot L, *et al*. Resting-State Connectivity of the Left Frontal Cortex to the Default Mode and Dorsal Attention Network Supports Reserve in Mild Cognitive Impairment. Frontiers in Aging Neuroscience. 2017; 9: 264. https://doi.org/10.3389/fnagi.2017.00264.
[51] van den Heuvel MP, Sporns O. Rich-club organization of the human connectome. The Journal of Neuroscience: the Official Journal of the Society for Neuroscience. 2011; 31: 15775–15786. https://doi.org/10.1523/JNEUROSCI.3539-11.2011.
[52] Kim DJ, Davis EP, Sandman CA, Sporns O, O'Donnell BF, Buss C, *et al*. Longer gestation is associated with more efficient brain networks in preadolescent children. NeuroImage. 2014; 100: 619–627. https://doi.org/10.1016/j.neuroimage.2014.06.048.
[53] Boot EM, Mc van Leijsen E, Bergkamp MI, Kessels RPC, Norris DG, de Leeuw FE, *et al*. Structural network efficiency predicts cognitive decline in cerebral small vessel disease. NeuroImage. Clinical. 2020; 27: 102325. https://doi.org/10.1016/j.nicl.2020.102325.
[54] Du J, Zhu H, Zhou J, Lu P, Qiu Y, Yu L, *et al*. Structural Brain Network Disruption at Preclinical Stage of Cognitive Impairment Due to Cerebral Small Vessel Disease. Neuroscience. 2020; 449: 99–115. https://doi.org/10.1016/j.neuroscience.2020.08.037.
[55] Cao R, Wang X, Gao Y, Li T, Zhang H, Hussain W, *et al*. Abnormal Anatomical Rich-Club Organization and Structural-Functional Coupling in Mild Cognitive Impairment and Alzheimer's Disease. Frontiers in Neurology. 2020; 11: 53. https://doi.org/10.3389/fneur.2020.00053.
[56] Xue C, Sun H, Hu G, Qi W, Yue Y, Rao J, *et al*. Disrupted Patterns of Rich-Club and Diverse-Club Organizations in Subjective Cognitive Decline and Amnestic Mild Cognitive Impairment. Frontiers in Neuroscience. 2020; 14: 575652. https://doi.org/10.3389/fnins.2020.575652.
[57] Chen H, Geng W, Shang S, Shi M, Zhou L, Jiang L, *et al*. Alterations of brain network topology and structural connectivity-functional connectivity coupling in capsular versus pontine stroke. European Journal of Neurology. 2021; 28: 1967–1976. https://doi.org/10.1111/ene.14794.
[58] Rosenberg GA. Binswanger's disease: biomarkers in the inflammatory form of vascular cognitive impairment and dementia. Journal of Neurochemistry. 2018; 144: 634–643. https://doi.org/10.1111/jnc.14218.
[59] Markus HS, de Leeuw FE. Cerebral small vessel disease: Recent advances and future directions. International Journal of Stroke: Official Journal of the International Stroke Society. 2023; 18: 4–14. https://doi.org/10.1177/17474930221144911.
[60] Benjamin P, Trippier S, Lawrence AJ, Lambert C, Zeestraten E, Williams OA, *et al*. Lacunar Infarcts, but Not Perivascular Spaces, Are Predictors of Cognitive Decline in Cerebral Small-Vessel Disease. Stroke. 2018; 49: 586–593. https://doi.org/10.1161/STROKEAHA.117.017526.